Tropical Atlantic Geostrophic Currents and Ship Drifts

SABINE ARNAULT

Laboratoire d'Océanographie Dynamique et de Climatologie/Office de la Recherche Scientifique et Technique Outre-Mer
Université Pierre et Marie Curie, Paris

Historical ship drifts and geostrophic surface currents obtained from hydrographic data are compared in the tropical Atlantic Ocean. The major components of the current system (North Equatorial Current, North Equatorial Countercurrent, South Equatorial Current) are clearly depicted by the two data sets. The main difference between the two fields is the weakness of the geostrophic currents except in the near-equatorial band, where on the contrary, they are much larger than the ship drifts. The amplitudes of the annual signals differ, but the phases are in rather good agreement. The uncertainty concerning the ship drift data, and the limitation of the geostrophic assumption, can explain a part of the differences encountered in this study. A much better comparison is obtained if we add to the geostrophic current u_g an Ekman drift current u_e computed from the climatological wind stress and a mean constant vertical viscosity value. Then the total velocity $u = u_g + u_e$ corresponds very closely in phase and amplitude to the ship drift velocity, except at the equator.

1. INTRODUCTION

A knowledge of the tropical ocean circulation is essential when considering climate problems. In tropical regions where heat storage is large, and in the vicinity of the equator where Coriolis acceleration vanishes, the transport of mass and heat intensifies at time scales of the order of months and years. The most striking and well known examples of correlation between climate events and ocean tropical circulation are found in the Pacific, especially during El Niño events [*Wyrtki*, 1977, 1979].

The oceanic circulation in tropical oceans consists of predominantly zonal currents in the oceanic interior and intense boundary currents near the coasts. This circulation is caused by the stress exerted upon the ocean surface by the trade winds over the Atlantic and Pacific, and the monsoons over the Indian Ocean. The surface current systems in the tropical Atlantic and Pacific Oceans have been observed for a long time, but although their mean structure is rather well known, their seasonal variability is still poorly described.

During 1982–1984 the French Programme Français Océan Climat en Atlantique Equatorial (FOCAL) and U.S. Seasonal Response of the Equatorial Atlantic (SEQUAL) experiment carried out an intensive field program to investigate the seasonal response of the tropical Atlantic Ocean to the wind forcing. During these experiments, surface drifters [*Richardson*, 1984; *Reverdin and McPhaden*, 1986], moored current meters, and periodic current profiler measurements [*Hisard and Hénin*, 1984] were used to observe surface and subsurface currents. A general description of the average seasonal variation of the circulation was needed to relate the limited 2-year measurements to climatology and, more generally, to compare with model results. However, the only earlier direct current measurements in the tropical Atlantic Ocean were too sparse and of too short duration to provide a basinwide view of the seasonal fluctuations of the surface current system [*Hisard*, 1973; *Bubnov and Yegorikhin*, 1977; *Halpern*, 1980]. As an alternative, we explored two different methods to get a large-scale representation of the surface circulation. The first uses the historical file of ship drift data. *Richardson and McKee* [1984], using these data to study the seasonal variation of the North Equatorial Countercurrent, concluded that the ship drift data give a clear and consistent picture of the surface current variations. The second method was to compute the geostrophic current from historical hydrographic data (conductivity-temperature-depth (CTD) profiles, Nansen bottle casts, mechanical bathythermographs (MBT), and expendable bathythermographs (XBT)). The hydrographic data have already been used to study the thermal structure of the tropical Atlantic Ocean [*Merle*, 1983; *Houghton*, 1983], the North Equatorial Countercurrent variability [*Garzoli and Katz*, 1983], and the seasonal variability of the surface dynamic topography [*Merle and Arnault*, 1985].

The focus of the present paper is on the analysis of the mean seasonal cycle of the surface currents in the tropical Atlantic Ocean by using the ship drift data set and the geostrophic/hydrographic data set. We will be particularly interested in comparing the two estimates of the currents and discussing whether the difference can be explained by Ekman drift.

The data and their processing are described in section 2. A comparative description of the seasonal variation of the surface current is given in section 3. Discussions are presented in section 4, and a summary and conclusions are found in section 5.

2. DATA AND PROCESSING

2.1. Ship Drift

The ship drift data set originates from the U.S. Naval Oceanographic Office and was generously provided to us by P. L. Richardson. It has been described by *Richardson and McKee* [1984] and consists of approximately 438,000 individual observations within the region bounded by 20°S–20°N, 10°E–70°W, and the coasts of Africa and South America.
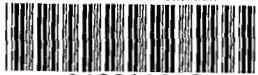
Richardson and McKee [1984] discussed many possible random and systematic errors which affect ship drift measurements. Each individual velocity measurement is estimated to have a random error of approximately 20 cm s⁻¹. Typical random errors of position, direction, and speed are ±2 km, ±1°, and ±0.3 knot (±15 cm s⁻¹).

Statistical analysis routines eliminated about 2% of the data as conspicuously erroneous. The resulting observations are not homogeneously distributed in space and time. Most ships followed standard sailing routes along which data den-

sity is higher than 500 observations per $2° \times 4°$ quadrangle (see Figure 1 of *Richardson and McKee* [1984]).

Most of the observations were collected between 1900 and 1976, with a significant decrease at the end of 1941. The data are very evenly distributed seasonally (see Figure 2 of *Richardson and McKee* [1984]), with a monthly average of about 30,000 observations.

In order to calculate and map the monthly mean velocity values between 16°S–20°N, 10°E–70°W, and the coasts of Africa and South America, individual velocity values were grouped into $2° \times 4°$ quadrangles. Monthly standard deviations of the currents from the ship drift data are given in Figure 1. The largest part of the basin has a deviation below 5 cm s^{-1} for both the zonal and meridional components. The largest standard deviations occur near the Brazilian coast, where the coastal currents are very strong; along the African coast; and in the South Atlantic, where data are scarce.

2.2. Hydrographic Data

The hydrographic data and their processing were described in a previous paper [*Merle and Arnault*, 1985]. We derived the dynamic height from a depth profile of temperature using a salinity interpolation. The salinity was interpolated from a local *T-S* relation. This method has been used successfully by *Emery* [1975] in the Pacific Ocean.

Two data sets were used: a temperature data set merging Nansen, MBT, and XBT data and a temperature-salinity-oxygen data set consisting of only the Nansen data.

The Nansen, MBT, and XBT data set contains approximately 140,000 temperature profiles between 16°S–30°N, 20°E–80°W, and the African and the South American coasts. Most of the profiles came from the National Oceanographic Data Center (NODC) data file, but additional bathythermographs from the French Navy and CTD casts from the oceanographic vessel *Capricorne* were also included. The file includes cruises from 1924 to 1978. The data distribution is irregular in time and space (see Figures 1 and 2 of *Merle and Arnault* [1985]); nevertheless, for the purpose of the large-scale study presented here, a monthly mean with a $2° \times 4°$ grid spacing has a sufficient number of observations in each box (over 30) to reduce the confidence interval of the mean to the order of 0.1°C. The monthly temperature was calculated at each standard level.

The Nansen temperature-salinity data set contains about 28,000 *T-S* profiles (see Figures 2 and 3 of *Merle and Arnault* [1985]). The $2° \times 4°$ grid spacing provided an annual mean *T-S* relation in each rectangle. We have not included the seasonal variability of the *T-S* relation. Thus in a given square and for a given month, the total error in the computation of the surface dynamic height relative to 500 dbar is the sum of the error which derives from the error in the mean temperature for each standard level and the error due to the neglect of the *T-S* seasonal variation. We finally concluded, after doing an error computation for a given region, that the total error of surface dynamic height relative to 500 dbar is close to ± 1 dyn cm [see *Merle and Arnault*, 1985].

Surface geostrophic velocities were then computed assuming the 500-dbar surface to be a level of no baroclinic motion. To compute these geostrophic currents, we used a numerical approximation of the derivative terms $\partial/\partial x$ and $\partial/\partial y$ given by the finite difference scheme

$$D'(i) = \frac{D(i+1) - D(i-1)}{2\Delta l}$$

where $D'(i)$ is the derivative term on grid point i, $D(i+1)$, $D(i-1)$ are the dynamic height on grid points $i+1$ and $i-1$, and Δl is the meridional or latitudinal distance between grid points $i+1$ and $i-1$. To estimate how the finite differentiation may reduce the real zonal geostrophic current, we will consider a sinusoidal geostrophic surface, $D(y) = \tilde{D}(\lambda) \cos [(2\pi/\lambda)y]$, where λ is the meridional wavelength. We have $D'(y) = -(2\pi/\lambda) \tilde{D}(\lambda) \sin [(2\pi/\lambda)y]$. In the numerical scheme, $D'(y)$ was estimated by

$$D_{num}'(y) = \frac{D(y + \Delta y) - D(y - \Delta y)}{2\Delta y}$$

$$= -\frac{\tilde{D}(\lambda)}{\Delta y} \sin \left(\frac{2\pi}{\lambda} y\right) \sin \left(\frac{2\pi}{\lambda} \Delta y\right)$$

Thus

$$\frac{D_{num}'(y)}{D'(y)} = \sin \left(\frac{2\pi}{\lambda} \Delta y\right) \bigg/ \frac{2\pi}{\lambda} \Delta y$$

Maps of mean annual surface dynamic heights [*Merle and Arnault*, 1985] show a succession of zonal ridges and lows separated by about 8° or 9° of latitude. So let us take $\lambda = 17°$ of latitude, Δy is 2° of latitude, which leads to a ratio of 0.91.

Because of the choice of $2° \times 4°$ boxes, the error in the dynamic height results in an anisotropic error in the geostrophic current which is for the zonal component as large as 18 cm s^{-1} at 1° from the equator, but only 3.5 cm s^{-1} at 5° of latitude and 1 cm s^{-1} at 15° of latitude; errors for the meridional component are 9, 1.8, and 0.5 cm s^{-1} at the same latitudes. We do not attempt to estimate geostrophic currents within 1° of the equator because of the large uncertainty.

3. RESULTS

3.1. Annual Mean Surface Currents in the Tropical Atlantic Ocean

The annual mean of the surface current obtained with the ship drift data is shown in Figure 2a. The major components of the tropical Atlantic surface current system are clearly identified. North of 10°N lies the westward flowing North Equatorial Current (NEC) with an average speed of more than 10 cm s^{-1}. Between 10°N and 4°N–6°N the North Equatorial Countercurrent (NECC) flows to the east against the trade winds, with an average speed of 15 cm s^{-1} increasing to 30 cm s^{-1} in the Guinea Current flowing south of the African coast. South of 4°N–6°N, the South Equatorial Current (SEC) flowing toward the west is intense and appears as the major component of the mean circulation, with speeds larger than 30 cm s^{-1}. West of 10°W, the SEC is divergent at the equator, and it divides into two separate jets. *Neumann* [1968] and *Richardson and McKee* [1984] noticed two maxima located at 2°N and 4°S. Near the American coast, the SEC intensifies and parallels the coast, dividing into northward and southward branches. Most of the flow runs northward along the coasts of Brazil, French Guiana, Surinam, Guyana, and Venezuela as the North Brazil and Guyana currents, with average speeds as high as 50 cm s^{-1}. The southward branch is weaker and clearly defined only south of 10°S. It is the starting point of the Brazil Current. There is no evidence of an eastward flow in the southern Atlantic similar to the NECC in the north, as was already noticed by *Richardson and McKee* [1984], at variance to previous studies [*Schumacher*, 1940, 1943; *Metcalf et al.*, 1962; *Molinari*, 1982]. This could be due either to windage effects on ship drift or to Ekman flow.
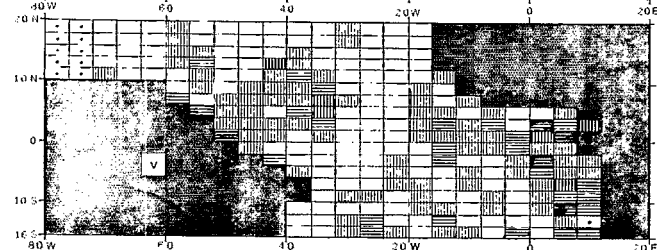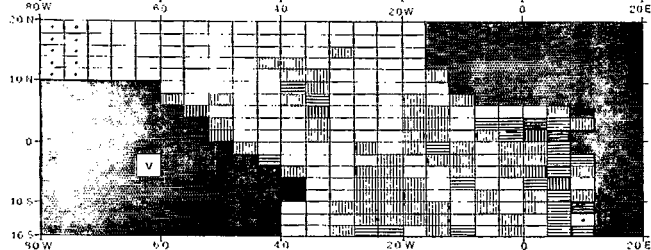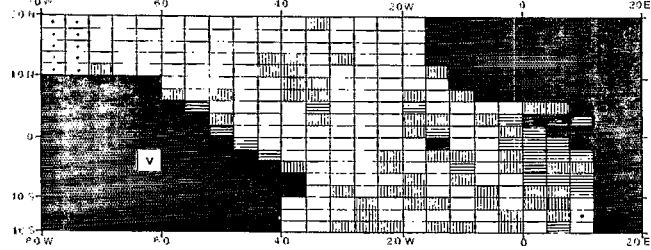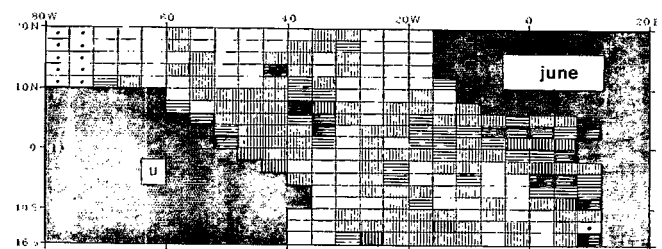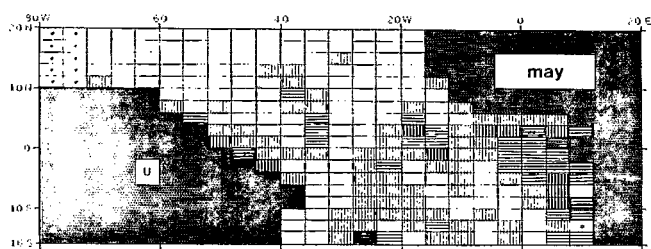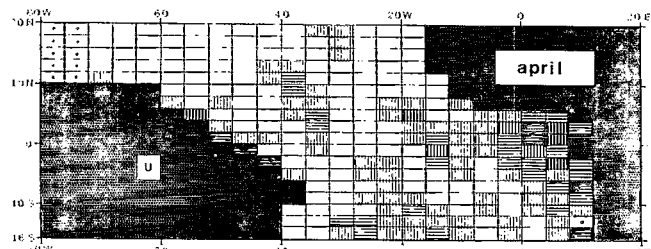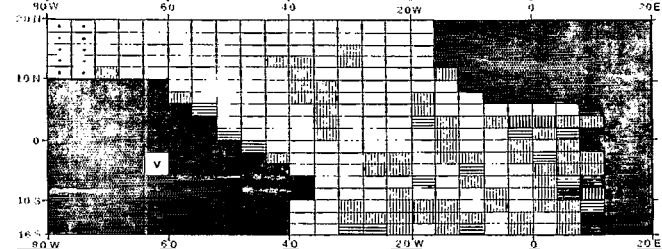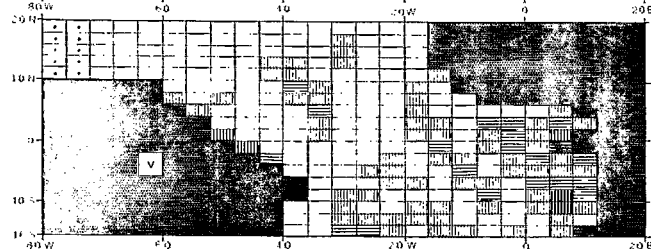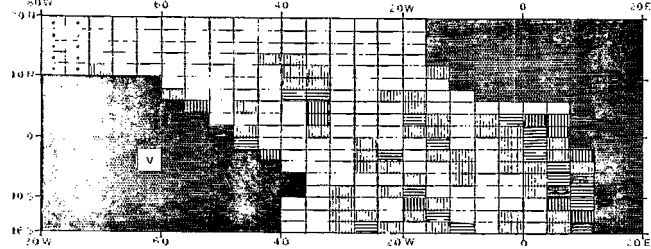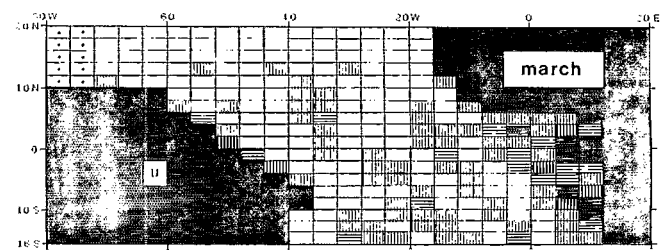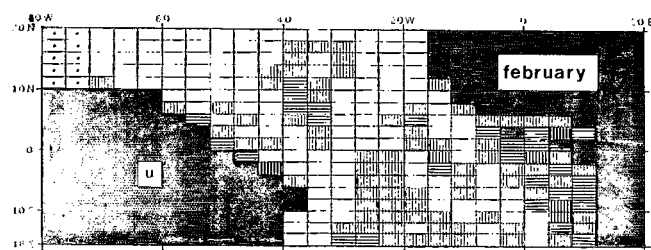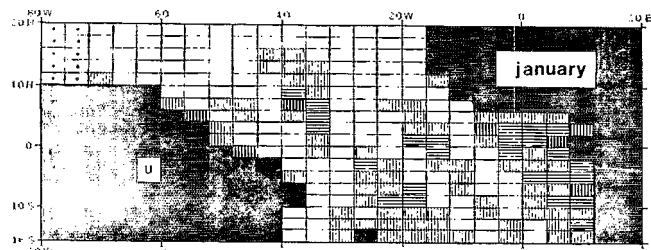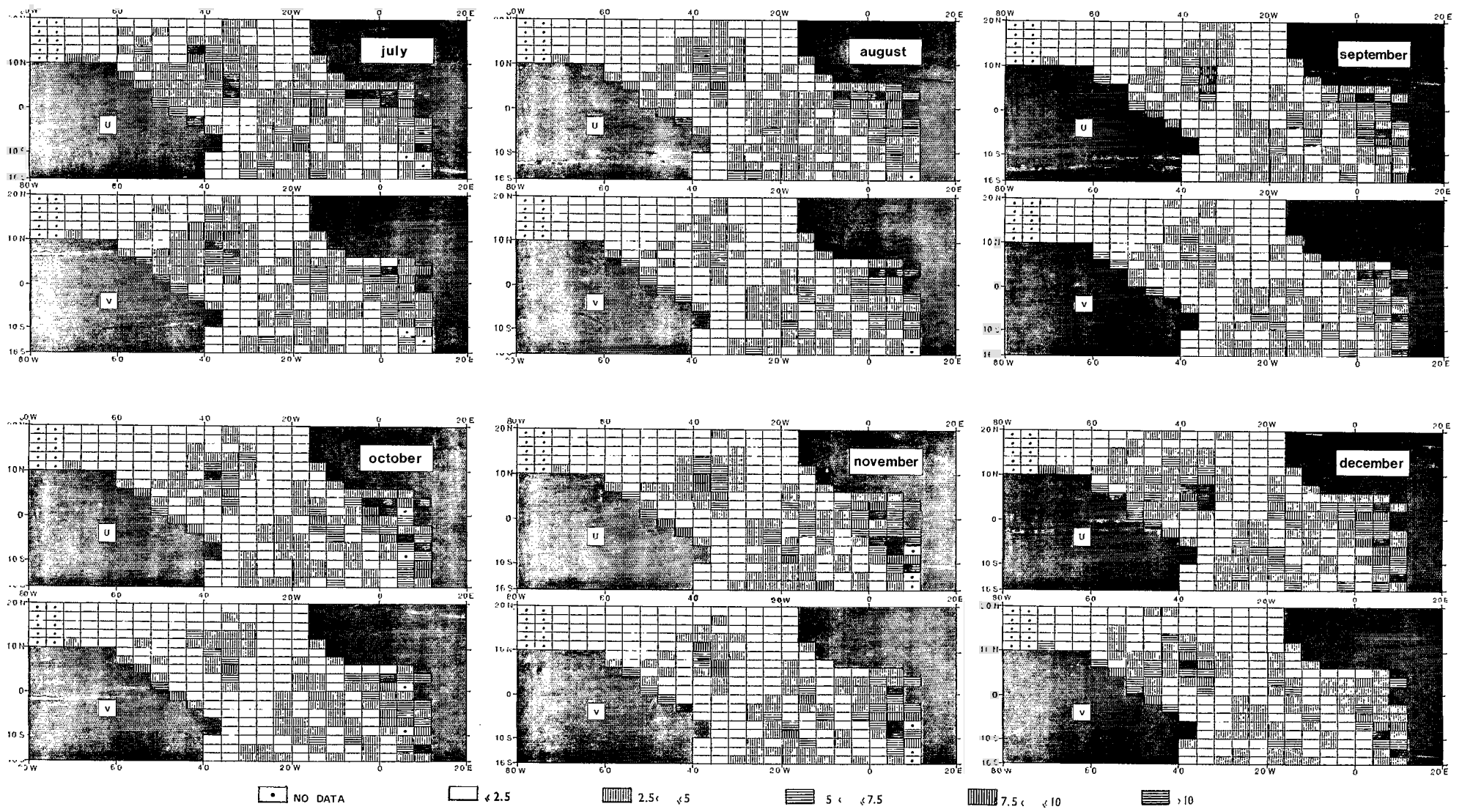
Fig. 1.   Monthly standard deviations of ship drifts (in centimeters per second).
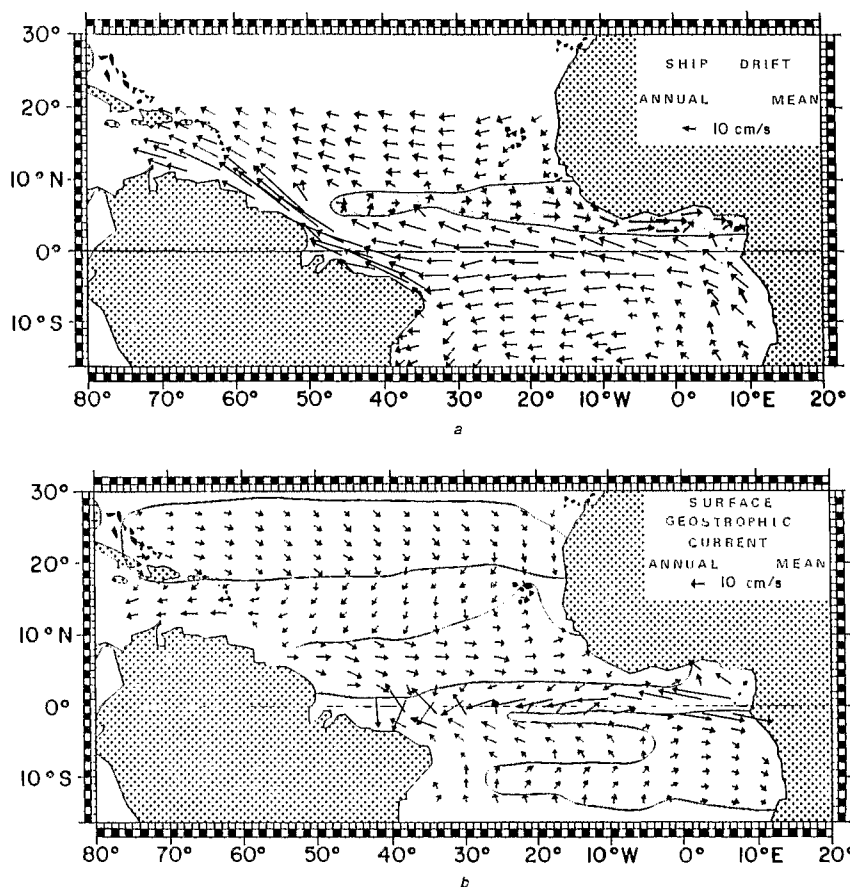
Fig. 2.   Mean annual surface (a) ship drift currents and (b) geostrophic currents (in centimeters per second).

The general pattern of the mean annual geostrophic current (Figure 2b) is rather different. In the upper part of the map, from 18°N to 30°N, the flow is eastward with uniform speed of less than 10 cm s^{-1}. South of 18°N the westward flowing NEC is clearly depicted west of 50°W. East of this longitude the current is primarily southward. The speeds are again less than 10 cm s^{-1}. South of 10°N, the eastward NECC attains its maximum value (approximately 10 cm s^{-1}) at 6°N–8°N. In the Gulf of Guinea the eastward current disappears east of 2°E. South of 4°N the geostrophic circulation is rather complex. North of the equator the flow is westward (SEC). Very close to the equator (1°N), the speed reaches more than 60 cm s^{-1}, and the western part of the basin has a strong southward geostrophic flow. South of the equator and west of 24°W the flow is still westward but with a strong northward component close to the equator. However, the eastern part of the south tropical Atlantic Ocean is, as a whole, covered by an eastward circulation of about 10 cm s^{-1} in the mean, but again larger in the vicinity of the equator. This South Equatorial Countercurrent (SECC) has been observed in the past [Schumacher, 1940, 1943; Metcalf et al., 1962; Molinari, 1982] and more recently during the FOCAL/SEQUAL experiment.

Thus the two sets of annual mean surface currents are different. The main difference is the weakness of the geostrophic current, except in the near-equatorial band where it is much larger than the ship drifts. The meridional component of the ship drift and geostrophic NEC are in opposite directions. The large spatial extent of the geostrophic NECC contrasts with the ship drifts, except in the Guinea Current. The two pictures clearly disagree in the SEC. There is an eastward geostrophic flow south of the equator (SECC) but no eastward flow in the

ship drift data. Finally, none of the coastal currents (North Brazil, Guyana, or Guinea currents) are correctly simulated in magnitude by the geostrophic computation.

3.2.   Seasonal Variability of the Surface Currents in the Tropical Atlantic Ocean

The major currents of the tropical Atlantic Ocean (NEC, NECC, and SEC) are roughly zonal. Thus to study their seasonal variation, we computed meridional averages for appropriate zones. We considered four meridional zones: (1) 12°N–18°N, (2) 4°N–8°N, (3) 1°N–2°N, and (4) 2°S–8°S. A north-south section of annual average zonal velocity in the central Atlantic shows that the NEC extends over box 1, the NECC extends over box 2, the northern SEC extends over box 3, and the southern SEC extends over box 4. Monthly sections still indicate the appropriateness of these latitudinal boundaries for the NEC, the SEC, and the core of the NECC despite its seasonal migration, so we will refer hereinafter to these meridional averages by the name of the main current usually present in the zone. Flows in certain coastal regions are also considered.

NEC.   Figures 3a and 3b present the month-longitude variation of the average zonal current in the NEC region for ship drift data and geostrophic currents. Both representations of the current intensify and do not exhibit a strong seasonal cycle along the American coast. In the center of the basin they vary in phase. They are most westward in boreal summer–fall and are less so in spring, but with a large difference in magnitude: the ship drift current is sometimes greater than 15 cm s^{-1} compared to 4 cm s^{-1} for the geostrophic NEC. In the east the ship drifts present eastward flow in July–August and
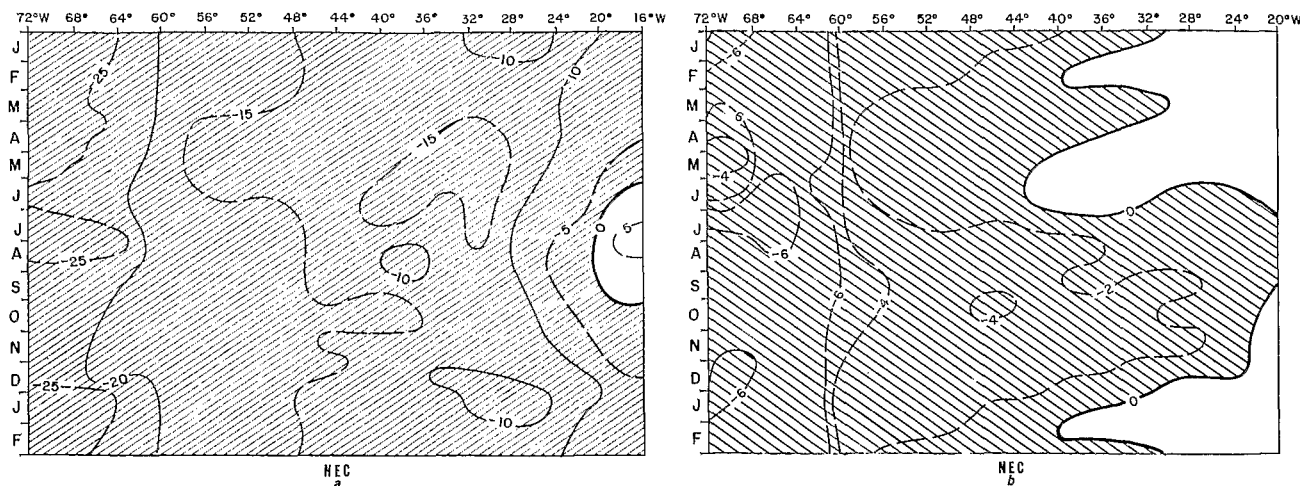
Fig. 3. (*a*) Longitude-time diagram of the zonal component of the ship drifts in the North Equatorial Current region averaged between 12°N and 18°N (in centimeters per second). Hatched areas denote westward current. (*b*) Same as Figure 3*a* for the geostrophic current.

strong NEC in May–June and November–December, whereas the geostrophic westward NEC is only defined from July to November–December with a maximum westward flow during boreal summer.

NECC. The ship drift data (Figure 4*a*) show an almost permanent and strong North Brazil Current flowing to the west from 50°W to the South American coast. It reaches a maximum speed of 70 cm s^{-1} from March to May. This current does not appear in the geostrophic computation (Figure 4*b*). Between 20°W and 48°W, the eastward NECC peaks in summer–fall at 20 cm s^{-1} for the geostrophic current and at 30 cm s^{-1} for the ship drift current. Maximum velocity at a given longitude occurs later as one moves west in both representations, but this peak in the geostrophic plot "propagates" westward faster (70 cm s^{-1} relative to 50 cm s^{-1} from ship drifts). From January to June the ship drifts change direction, whereas the geostrophic current reverses only slightly in April–May and then only in the west. This reversal has been observed with different data sets and with different amplitudes

[*Richardson and McKee*, 1984; *Garzoli and Katz*, 1983]. East of 20°W, there are two maxima of eastward flow (August to October and January to February) in the geostrophic signal which are not evidenced by the ship drift current's single maximum in July.

Northern SEC. In the ship drift data (Figure 5*a*), there is again a strong North Brazil Current peaking between 44°W and 48°W in July and August. In contrast, the geostrophic current (Figure 5*b*) is eastward in the western part of the basin from February to June. In the central part of the basin, the currents fluctuate almost in phase. The ship drifts indicate strong northern SEC in June–July (more than 50 cm s^{-1}) and December (40 cm s^{-1}); the geostrophic SEC reaches 90 cm s^{-1} in June–July and 40 cm s^{-1} in November–December. Thus the geostrophic current is stronger than the ship drift current. The velocity contours also suggest the presence of a westward phase propagation with a speed of $\simeq 1$ m s^{-1}. In the east, both representations of the current fluctuate with a semiannual period, with maximum westward flow in May–June (50
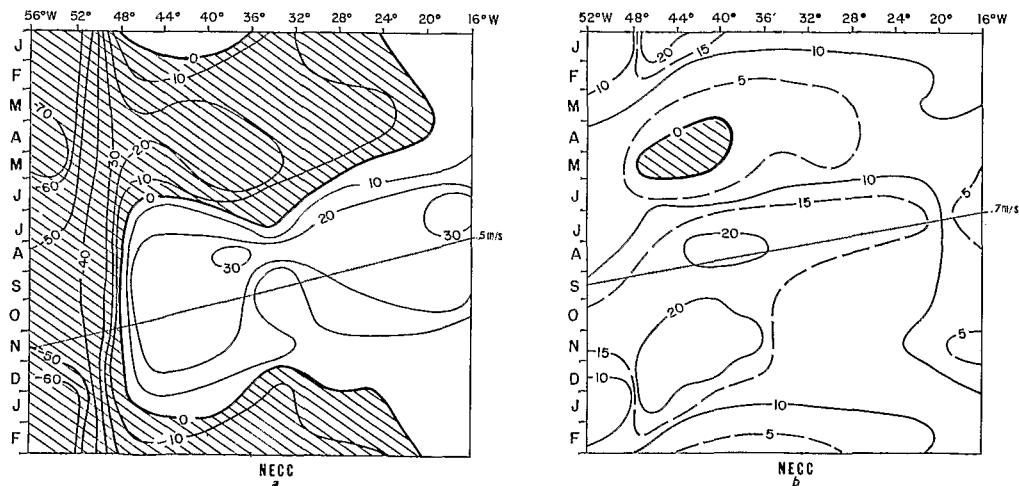

Fig. 4. (*a*) Longitude-time diagram of the zonal component of the ship drifts in the North Equatorial Countercurrent region averaged between 4°N and 8°N (in centimeters per second). Hatched areas denote westward current. (*b*) Same as Figure 4*a* for the geostrophic current.
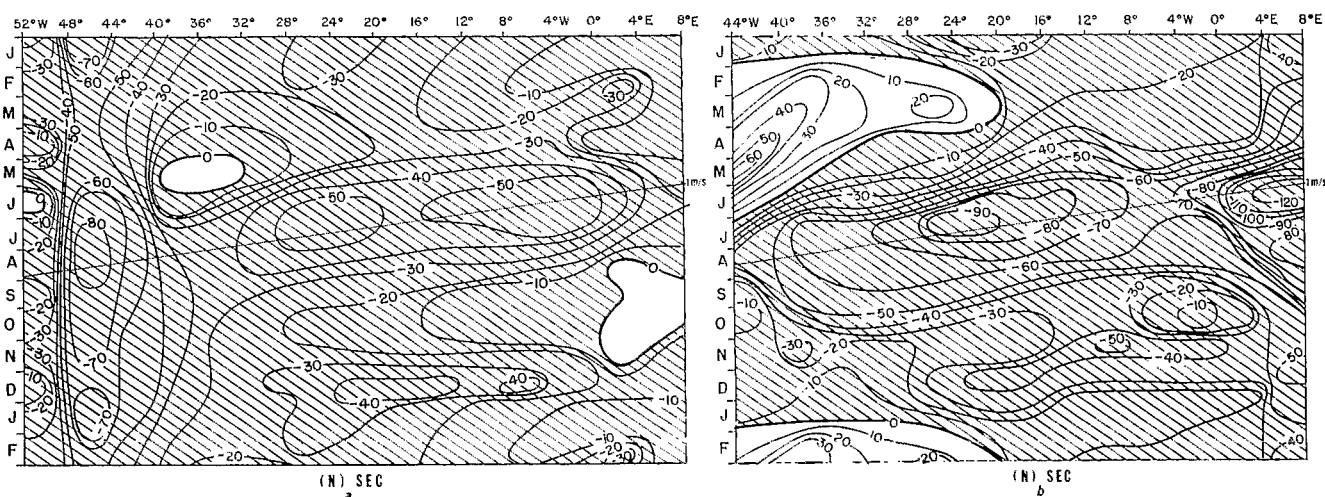
Fig. 5. (a) Longitude-time diagram of the zonal component of the ship drifts in the northern South Equatorial Current region averaged between 1°N and 2°N (in centimeters per second). Hatched areas denote westward current. (b) Same as Figure 5a for the geostrophic current.

cm s⁻¹) and November–December (20 cm s⁻¹) for the ship drifts and in June (120 cm s⁻¹) and December (50 cm s⁻¹) for the geostrophic current.

Southern SEC. In this region, ship drifts present a permanent westward southern SEC (Figure 6a), whereas the geostrophic current (Figure 6b) shows an eastward flow in the Gulf of Guinea most of the time. In the west the ship drift coastal current peaks during the early boreal summer (≃ 60 cm s⁻¹). Between 28°W and 36°W, the geostrophic current reaches more than 10 cm s⁻¹ in spring and summer. In the central part of the basin the currents have smaller month to month fluctuations than the northern SEC and appear to be dominated by an annual period, with a maximum westward flow in June–July of 30 cm s⁻¹ for the ship drifts and 10 cm s⁻¹ for the geostrophic current. In the east the westward ship drift current peaks in May–June and November. The eastward geostrophic current reaches maximum values in February–March and September–October. This eastward circulation seems to be consistent with various observations in the same region [*Reid*, 1964], but drift buoys indicate a dominant west-

ward current in this area [*Molinari*, 1982; *Reverdin and McPhaden*, 1986].

Coastal boundary currents. The ship drift maps present strong coastal currents near the continental boundaries along the American and African coasts which the geostrophic maps do not reproduce.

In the ship drift data, the zonal Guinea Current is well developed between 2°N and the coast north of the Gulf of Guinea (Figure 7). It forms the continuation of the NECC in the Gulf of Guinea. It can be followed up to 8°E in agreement with earlier observations [*Lemasson and Rebert*, 1973]. A strong maximum (60 cm s⁻¹) appears between 4°E and 8°W in July–August. A secondary maximum is also observed in February (40 cm s⁻¹).

The North Brazil Current and the Guyana Current (10°N, 58°W to 6°S, 32°W) are strong with a large meridional component. The seasonal variation of the speed of these currents (Figure 8) has a large maximum from July to October in the middle of the section (1 m s⁻¹). off the mouth of the Amazon river. Off Recife-Natal the maximum (50–60 cm s⁻¹) is ob-
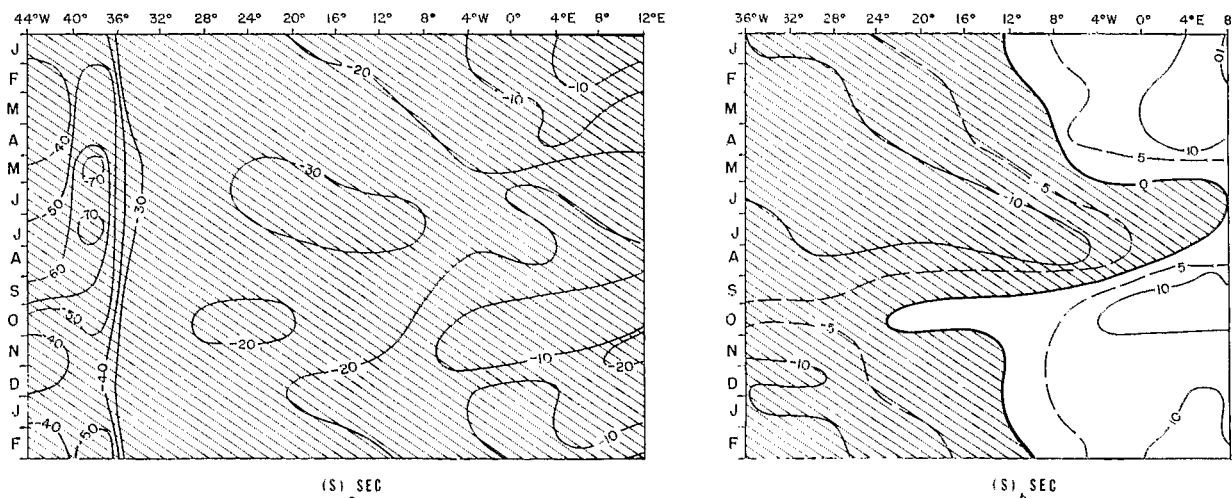

Fig. 6. (a) Longitude-time diagram of the zonal component of the ship drifts in the southern South Equatorial Current region averaged between 2°S and 8°S (in centimeters per second). Hatched areas denote westward current. (b) Same as Figure 6a for the geostrophic current.
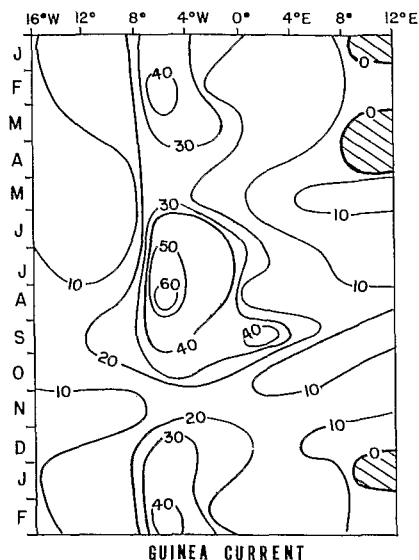
Fig. 7. Longitude-time diagram of the zonal component of the ship drifts in the Guinea Current region averaged between 2°N and 6°N (in centimeters per second). Hatched areas denote westward current.

served in late boreal spring (May–June). Off French Guiana the maximum speed (50 cm s^{-1}) is reached in early spring (April).

4. DISCUSSION

This first extensive comparison of the seasonal variation of the geostrophic and ship drift currents reveals large differences in the magnitude of the currents and in the amplitude of their seasonal variations. Nevertheless, the phases are in good agreement. These differences and similarities need to be discussed if we want to understand the actual surface currents.

We will first consider the source of uncertainty concerning the ship drift data and then discuss the limitation of the geostrophic assumption.

As was mentioned earlier and as was explained by *Rich-*

ardson and McKee [1984], a ship drift measurement of surface current velocity is the difference between the velocity of the ship determined from two position fixes and an estimate of the average velocity of the ship through the water during time intervals of usually 6, 12, or 24 hours. Each measurement is an average over the depth of the ship's hull and along the ship's path between fixes. Thus only large-scale features greater than a few hundred kilometers can be seen. This could explain the differences observed between ship drift currents and current meter data, for example. In addition, the averaging used for this study could explain the absence of the eddy structures near the American coast which were observed during the FOCAL/SEQUAL experiment [*Bruce and Kerling*, 1984]. Another source of difficulty in interpreting the ship drift currents is due to the ship's hull. Profiles of zonal currents presented by *Halpern* [1980] in the Atlantic NECC showed a shear of about 10 cm s^{-1} in the first 30 m, and even larger shears may occur. Thus ship drift data will differ from the actual surface current.

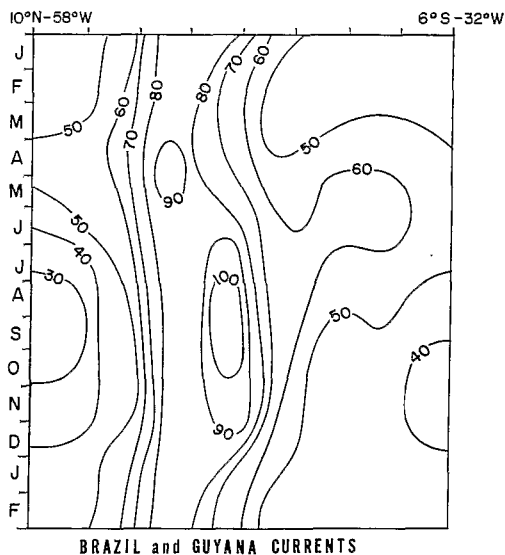*Richardson and McKee* [1984] suggested that windage ef-

Fig. 8. Seasonal evolution of the ship drift magnitude in the North Brazil and Guyana current region along the American coast between 6°S, 32°W and 10°N, 58°W (in centimeters per second).
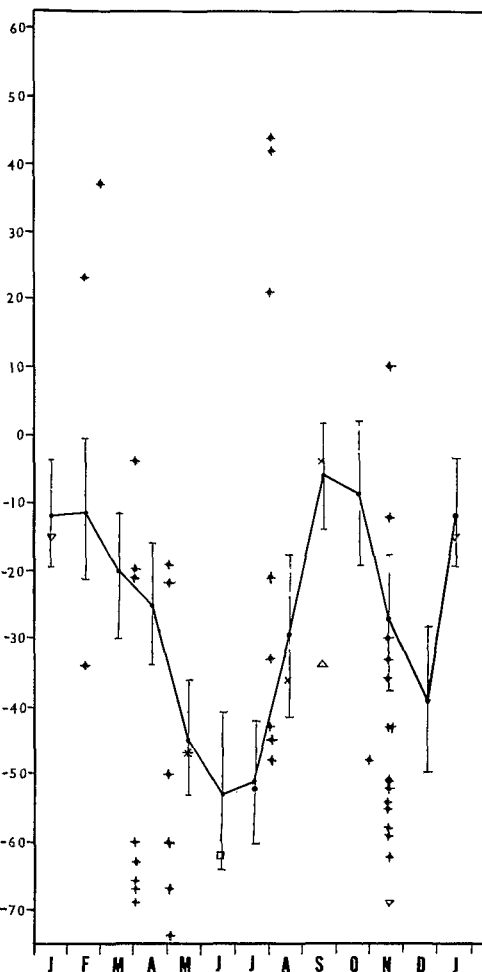

Fig. 9. Comparison of the zonal component of the ship drift data (in centimeters per second) with direct measurements in the 0°–8°W, 2°N–2°S region. Error bars on ship drifts are indicated by vertical lines. Direct measurements are from R/V *Capricorne*, ORSTOM cruises 7302 and 7107 (inverted triangles); R/V *Capricorne*, FOCAL 0-8 (pluses); R/V *Zvezda*, 14 and 15 (Atlantic Niño) (crosses); R/V *Geronimo*, Equatorial Atlantic Survey (EQUALANT) 3 (triangles); R/V *Professor Albrecht Penck* (asterisks); R/V *Jean Charcot*, Guinée 1, ORSTOM (squares).
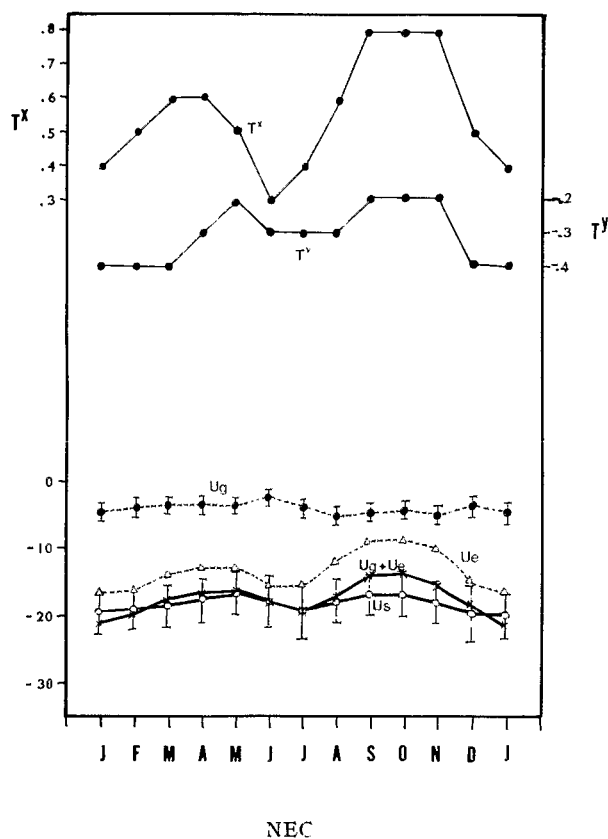
NEC

Fig. 11. Comparison of the annual cycle of the zonal component of the current in the North Equatorial Current region averaged in the region $12°N-18°N$, $40°W-72°W$ obtained by ship drift data (u_s, solid line), by geostrophy (u_g, dashed line), by Ekman drift (u_e, dashed line), and by summing the Ekman and geostrophic component ($u_g + u_e$, solid line). Values are in centimeters per second. Vertical lines indicate error bars.

rents, we have computed average zonal velocities, for the ship drifts u_s, the geostrophic current u_g, and the Ekman current u_e in four boxes: (1) NEC ($12°N-18°N$, $40°W-72°W$), (2) NECC ($4°N-8°N$, $16°W-48°W$), (3) northern SEC ($1°N-2°N$, $0°-40°W$), and (4) southern SEC ($2°S-8°S$, $36°W-8°E$). These boxes do not include coastal currents, since as we remarked earlier, finite difference scheme and initial averaging account for a large part of the differences between geostrophic and ship drift coastal currents.

NEC. The directly wind-driven ageostrophic component of the NEC (Figure 11) follows the seasonal cycle of the wind stress with a bimodal signal: it is least in March–April and in September–October (10 cm s^{-1}), and greatest in June–July and January–February (15 cm s^{-1}). The range of the annual Ekman signal is greater than that of the ship drift or the geostrophic signal. When added to the geostrophic component, there is a remarkable quantitative and in-phase agreement between this sum and the ship drift current during the first 6 months of the year (January–July). The sum results in a second extremum (a minimum in speed) in October larger than the one observed in the ship drift data. The difference, however, falls within the error bars.

NECC. The mean Ekman flow in this region (Figure 12) is westward during the 8 months of the year from November to June. This westward current peaks in January–February (more than 20 cm s^{-1}). The Ekman flow in the NECC is a

maximum in August ($\simeq 10$ cm s^{-1}). The main disagreement between the ship drifts and the geostrophic current in this region is the reversal in the west of the usual eastward current, but owing to the large westward Ekman flow, the sum of the geostrophic and the Ekman components now almost perfectly reproduces the annual cycle of the zonal ship drift current.

Northern SEC. As we remarked earlier for the geostrophic assumption, we expect poorer agreement in this band due to the proximity of the equator where the Coriolis parameter vanishes. We note (Figure 13) that the problems concerning the magnitude of the currents and the annual amplitude remain when the Ekman component is added, but that differences are now reduced.

Southern SEC. The mean value of the Ekman flow in the SEC (Fig. 14) is now close to the ship drift current ($\simeq 20$ cm s^{-1}). It is a maximum in July–August (more than 20 cm s^{-1}), but it is difficult to see a secondary maximum in October–November. The amplitude of the annual signal for $u_e + u_g$ is stronger than for the ship drift current u_s because of the sum's large value in August. During the rest of the year, the currents are in rather good agreement.

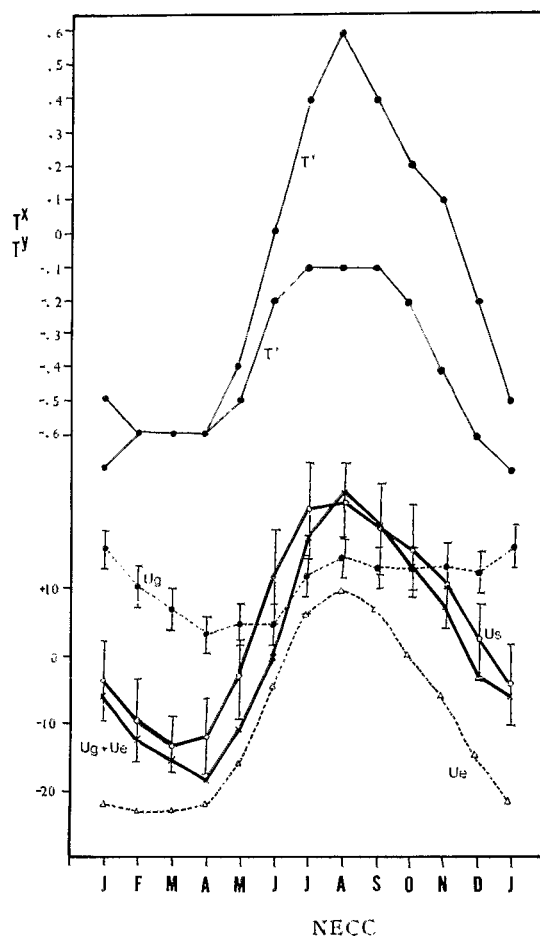We must keep in mind that the Ekman drift computation

NECC

Fig. 12. Comparison of the annual cycle of the zonal component of the current in the North Equatorial Countercurrent region averaged in the region $4°N-8°N$, $16°W-48°W$ obtained by ship drift data (u_s, solid line), geostrophy (u_g, dashed line), Ekman drift (u_e, dashed line), and by summing the Ekman and geostrophic component ($u_g + u_e$, solid line). Values are in centimeters per second. Vertical lines indicate error bars.
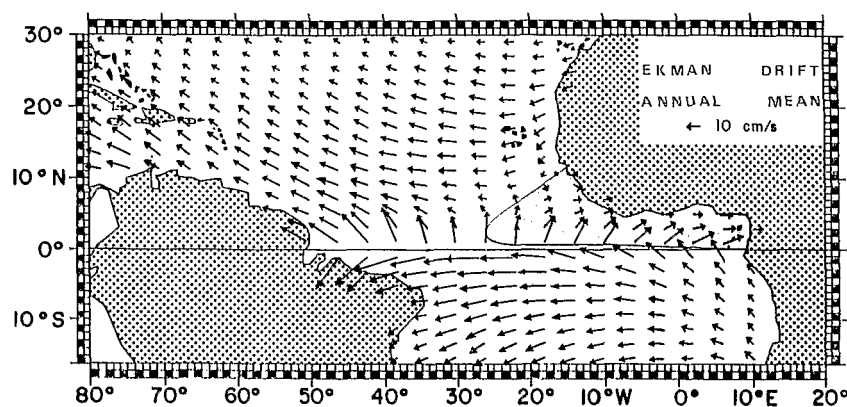
Fig. 10. Mean annual Ekman surface current (in centimeters per second).

fects on the ships could lead to systematic errors in surface velocity. It is difficult to assess the leeway effect on the historical ship drift data set because leeway depends heavily on the particular ship's design, its speed, and its course relative to the wind. We can only reasonably think that this tends to cause overestimation of the SEC speed and absence of SECC.

All these sources of uncertainty can explain part of the difference encountered between ship drift data and direct current measurements such as those obtained by profilers. Comparing the ship drift current with direct current observations could be very instructive wherever it is possible, as is the case in the Gulf of Guinea around the equator between 0° and 8°W (Figure 9). We first observe that the amplitude of the annual signal is larger than the monthly error bars and is therefore significant. Second, we can see that this signal is in agreement with those given by direct measurements.

The limitations of the geostrophic assumption are numerous. As we explained earlier, the numerical scheme chosen to calculate the geostrophic current reduces the signal by about 10%. This can explain a small part of the smaller amplitude of annual signal in the geostrophic estimate compared with the ship drift current.

Independent of this numerical problem, the initial averaging by $2° \times 4°$ quadrangles certainly explains why narrow coastal currents such as the North Brazil or Guinea Currents are not resolved by the geostrophic computation.

Another assumption made for geostrophic current computations is the level of no motion. We have chosen 500 dbar as our reference surface and therefore assumed that 500 dbar is a level of no motion. Defant [1941] also suggested this level for geostrophic computation in the western Atlantic between 15°N and 5°S. Wyrtki [1974] found it adequate for computations in the tropical regions. Direct current measurements at this depth to verify this assumption are rare. Weisberg et al. [1979] reported two measurements at 500 m from the equator and 26°W and 28°W during the GARP Atlantic Tropical Experiment (GATE) in 1974. The zonal/meridional component averages for 48 and 40 days, respectively, were 0.1/8.5 and 0.3/−2.8 cm s^{-1}. So our assumption, for a large-scale variability study of surface current such as the one presented here, may be better for the zonal than for the meridional current.

In fact, none of the limitations of the ship drift data, nor of the geostrophic computation, can explain the major differences noticed between these two representations of the current. Some of them contribute a part to the disagreement, but

in order to explain all of the differences, we have to take into account other physical processes.

A scaling in the horizontal momentum equations (see, for example, Pond and Pickard [1978]) shows that if we decompose u as the sum of a geostrophic component u_g plus an Ekman component u_e plus a residual term u_r, the residual term is only important for the currents very close to the equator, such as the northern SEC.

We noticed earlier that the ship drift data give a rather consistent portrayal of the tropical Atlantic surface circulation (Figure 9). We now investigate if the differences encountered between ship drifts and geostrophic currents are due to Ekman drift.

We computed this Ekman drift as suggested by Halpern's [1979] observations in the Pacific NECC. The wind stresses were obtained from the Hellerman and Rosenstein [1983] file. They consist of climatological monthly means of wind stresses by $2° \times 2°$ square. We take the water density to be 10^3 kg m^{-3} and the vertical viscosity A_z to be equal to 10^{-2} m^2 s^{-1}. Values for A_z in the ocean vary from 10^{-5} to 10^{-1} m^2 s^{-1} [Pond and Pickard, 1978]. Measurements show that these parameters vary considerably in the tropical ocean. They usually have large values in the mixed surface layer but have very small values below the thermocline [Pacanowski and Philander, 1981; Gregg et al., 1985]. Crawford and Osborn [1979a, b] suggested that in the Atlantic 13°C thermostad, A_z varies from 2 to 11×10^{-4} m^2 s^{-1}. At the core of the undercurrent, the value is of the order of 10^{-4} m^2 s^{-1}, and above the core it varies from 8 to 100×10^{-4} m^2 s^{-1}. Jones [1973] and Gregg [1976] reached the same conclusion in the Pacific Ocean. In the equatorial Pacific again, Bryden and Brady [1985], using North Pacific Experiment (NORPAX) and Equatorial Pacific Ocean Climate Studies (EPOCS) data found a value of 1.66 $\times 10^{-3}$ m^2 s^{-1} at 150°W. Halpern [1980] found A_z from 3 to 10×10^{-3} m^2 s^{-1} in the mixed layer near 8°N, 23°W. Thus our choice belongs to this range of values, being at the higher end. Here again we stopped our computations at 1° from the equator.

The annual mean of the Ekman drift (Figure 10) is generally westward except in the Gulf of Guinea along the northern African coast, where the eastward NECC and Guinea Current are distinguishable. Along the equator, the Ekman flow is strongly divergent in the west.

To determine whether the Ekman drift can explain the differences encountered between ship drifts and geostrophic cur-

depends on the vertical exchange coefficient. It appears as an inverse square root in the computation of the zonal component. We chose $A_z = 10^{-2}$ m^2 s^{-1} as a mean value. The Ekman current's direction and its seasonal variability are not dependent on this choice, but its mean value is affected. As we have seen earlier. the vertical exchange coefficient may range from 10^{-1} to 10^{-5} m^2 s^{-1} [*Pond and Pickard*, 1978] for the global ocean, but values for the tropical mixed layer surface are between 10^{-3} and 10^{-2} m^2 s^{-1} [*Halpern*, 1980; *Crawford and Osborn*, 1979a; *Jones*, 1973; *Gregg*, 1976]. The values of Ekman zonal velocity corresponding to 10^{-3} m^2 s^{-1} will change our computation by a factor of 3. What is noteworthy here is that a rough choice of the mean value (10^{-2} m^2 s^{-1}) for A_z gives a good result. It seems likely that the real surface current of the central tropical Atlantic Ocean is principally the sum of a geostrophic and an Ekman component and that the ship drift current correctly represents this sum except for a band very close to the equator (2°N–2°S).

5. SUMMARY AND CONCLUSIONS

The purpose of this study is to describe the seasonal variability of the tropical Atlantic surface currents using two differ-
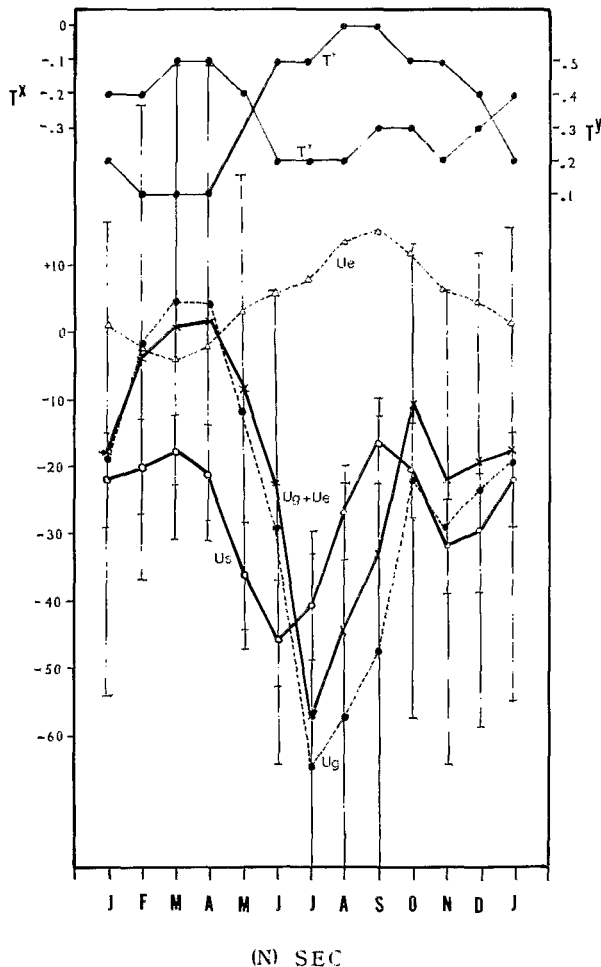

(S) SEC

Fig. 14. Comparison of the annual cycle of the zonal component of the current in the southern South Equatorial Current region averaged in the region 2°S–8°S. 36°W–8°E obtained by ship drift data (u_s, solid line), geostrophy (u_g, dashed line), Ekman drift (u_e, dashed line), and by summing the Ekman and geostrophic component ($u_g + u_e$, solid line). Values are in centimeters per second. Vertical lines indicate error bars.
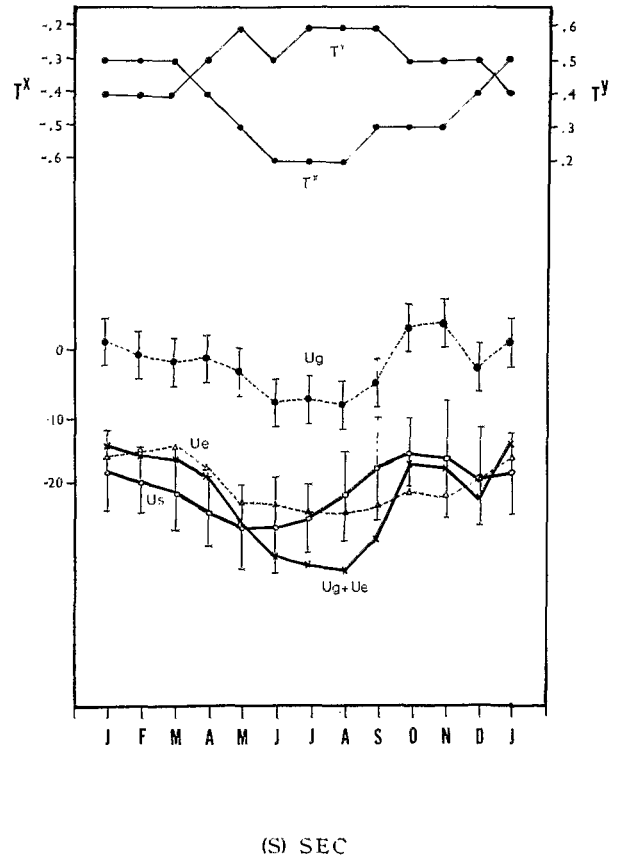

(N) SEC

Fig. 13. Comparison of the annual cycle of the zonal component of the current in the northern South Equatorial Current region averaged in the region 1°N–2°N. 0°–40°W obtained by ship drift data (u_s, solid line), geostrophy (u_g, dashed line), Ekman drift (u_e, dashed line), and by summing the Ekman and geostrophic component ($u_g + u_e$, solid line). Values are in centimeters per second. Vertical lines indicate error bars.

ent data sets: ship drifts and geostrophic currents obtained from hydrographic data.

Ship drifts give a rather clear and consistent picture of the surface circulation in the tropical Atlantic Ocean. In the open ocean, three main currents are present. The westward North Equatorial Current, between 12°N and 18°N, peaks (15 cm s^{-1}) in boreal summer and weakens (10–12 cm s^{-1}) in spring and fall. The eastward North Equatorial Countercurrent, between 4°N and 8°N, strengthens (20 cm s^{-1}) in boreal summer and reduces in spring. Most of the western part of the current reverses during the first months of the year. The westward South Equatorial Current has its northern branch (1°N–2°N) greatest (more than 40 cm s^{-1}) in early boreal summer and November (30 cm s^{-1}), and least in spring and early fall (15–20 cm s^{-1}). Its southern branch (2°S–8°S) is also strongest two times a year. in early boreal summer (25 cm s^{-1}) and in December (less than 20 cm s^{-1}). Its diminution occurs in autumn (15 cm s^{-1}).

Two coastal currents are clearly seen. The Guinea Current, which is a continuation of the North Equatorial Countercurrent in the Gulf of Guinea. peaks in boreal summer (60 cm s^{-1}) and weakens in spring and late fall. The North Brazil and Guyana currents. which flow along the northern Brazilian coast, have a maximum intensity in boreal spring at their southernmost part. in summer and fall for their central part,

and in spring again for their northernmost part. Despite the problems associated with the interpretation of ship drift data (wind effect and averages over ship's hull and ship's path), this representation of the surface current system in the tropical Atlantic Ocean is in agreement with direct measurements obtained during different cruises. The seasonal variability is also reproduced well.

The geostrophic currents confirm these mean structures and their seasonal variability, except for the coastal currents (presumably because of the averaging and finite difference scheme used in the computations). There are, however, important disagreements in magnitude with the ship drift currents. The geostrophic current is generally too weak and has a seasonal range too small, compared with the ship drift data. Close to the equator, on the other hand, the effect of the geostrophic assumption could explain the large geostrophic current compared with the ship drift current, particularly in the northern South Equatorial Current. Other differences can be due to the errors inherent in both data sets. This is especially true of the geostrophic current, where the assumption of the level of no motion can introduce an error in the computation of the North Equatorial Current and North Equatorial Countercurrent. Also of concern is the spatial discretization, which can affect the amplitude of the geostrophic annual signal by reducing the estimated current.

A much better comparison is found when we add to the geostrophic current an Ekman drift current computed using a climatological wind stress [Hellerman and Rosenstein, 1983] and a mean vertical viscosity. Then the velocity $\mathbf{u} = \mathbf{u}_g + \mathbf{u}_e$ is very close to the ship drift off the equator.

Thus for a large-scale study of the tropical Atlantic surface current, ship drift data, wind measurements, and hydrological data provide a reasonably complete and consistent picture of the surface circulation and its seasonal variability. We expect further progress when more precise and detailed data sets are available after the processing of the FOCAL/SEQUAL data set for the years 1982–1984.

REFERENCES

Bruce, J. G., and J. L. Kerling, Near equatorial eddies in the North Atlantic, *Geophys. Res. Lett., 11*, 779–782, 1984.

Bryden, H. L., and E. C. Brady, Diagnostic model of the three-dimensional circulation in the upper equatorial Pacific Ocean, *J. Phys. Oceanogr., 15*, 1255–1273, 1985.

Bubnov, V. A., and V. D. Yegorikhin, Investigation of the large scale current structure in the tropical Atlantic Ocean along 23°30'W, *Oceanology, Engl. Transl., 17*(6), 631–635, 1977.

Crawford, W. R., and T. R. Osborn, Microstructure measurements in the Atlantic Equatorial Undercurrent during GATE, *Deep Sea Res., 26*, suppl. 2, 285–308, 1979a.

Crawford, W. R., and T. R. Osborn, Energetics of the Atlantic equatorial currents, *Deep Sea Res., 26*, suppl. 2, 309–324, 1979b.

Defant, A., Quantitative Untersuchungen zur Statik und Dynamik des Atlantischen Ozeans, *Meteor Exped., 6*, 190–260, 1941.

Emery, W. J., Dynamic height from temperature profiles, *J. Phys. Oceanogr., 5*, 369–375, 1975.

Garzoli, S. L., and E. J. Katz, The forced annual reversal of the Atlantic North Equatorial Countercurrent, *J. Phys. Oceanogr., 13*, 2082–2090, 1983.

Gregg, M. C., Temperature and salinity microstructure in the Pacific Equatorial Undercurrent, *J. Geophys. Res., 81*(6), 1180–1196, 1976.

Gregg, M. C., H. Peters, J. C. Wesson, N. S. Oakey, and T. J. Shay, Intensive measurements of turbulence and shear in the equatorial undercurrent, *Nature, 318*, 140–144, 1985.

Halpern, D., Observations of upper ocean currents at DOMES sites A, B and C in the tropical central North Pacific Ocean during 1975 and 1976, in *Marine Geology and Oceanography of Pacific Manganese Nodule Province*, edited by J. L. Bischoff and D. Z. Piper, pp. 43–82, Plenum, New York, 1979.

Halpern, D., Variability of near surface currents in the Atlantic North Equatorial Countercurrent during GATE, *J. Phys. Oceanogr., 10*, 1213–1220, 1980.

Hellerman, S., and M. Rosenstein, Normal monthly wind stress over the world ocean with error estimates, *J. Phys. Oceanogr., 13*, 1093–1104, 1983.

Hisard, P., Variations saisonnières à l'équateur dans le Golfe de Guinée, *Cah. ORSTOM, Ser. Oceanogr., 12*(3), 349–358, 1973.

Hisard, P., and C. Hénin, Zonal pressure gradient, velocity and transport in the Atlantic equatorial undercurrent from FOCAL cruises (July 1982–February 1984), *Geophys. Res. Lett., 11*, 761–764, 1984.

Houghton, R. W., Seasonal variations of the subsurface thermal structure in the Gulf of Guinea, *J. Phys. Oceanogr., 13*, 2070–2081, 1983.

Jones, J. H., Vertical mixing in the Equatorial Undercurrent, *J. Phys. Oceanogr., 3*, 286–296, 1973.

Lemasson, L., and J. P. Rebert, Circulation dans le Golfe de Guinée, Etude de la région d'origine du sous courant ivoirien, *Cah. ORSTOM, Ser. Oceanogr., 11*(3), 303–316, 1973.

Merle, J., Seasonal variability of the subsurface thermal structure in the tropical Atlantic Ocean, in *Hydrodynamics of the Equatorial Ocean*, edited by J. C. J. Nihoul, pp. 31–49, Elsevier, New York, 1983.

Merle, J., and S. Arnault, Seasonal variability of the surface dynamic topography in the tropical Atlantic Ocean, *J. Mar. Res., 43*(2), 267–288, 1985.

Metcalf, W. G., A. D. Voorhis, and M. C. Stalcup, The Atlantic equatorial undercurrent, *J. Geophys. Res., 67*(6), 2499–2508, 1962.

Molinari, R. L., Observations of eastward currents in the tropical South Atlantic Ocean: 1978–1980, *J. Geophys. Res., 87*(C12), 9707–9714, 1982.

Neumann, G., *Ocean Currents*, Elsevier, New York, 1968.

Pacanoswki, R. C., and S. G. H. Philander, Parameterization of vertical mixing in numerical models of tropical oceans, *J. Phys. Oceanogr., 11*, 1443–1451, 1981.

Pond, S., and G. L. Pickard, *Introductory Dynamic Oceanography*, 241 pp., Pergamon, New York, 1978.

Reid, J. L., Evidence of South Equatorial Countercurrent in the Atlantic Ocean in July 1963, *Nature, 203*(4941), 182, 1964.

Reverdin, G., and M. McPhaden, Near-surface current and temperature variability observed in the equatorial Atlantic from drifting buoys, *J. Geophys. Res., 91*(C5), 6569–6582, 1986.

Richardson, P. L., Drifting buoy trajectories in the Atlantic North Equatorial Countercurrent during 1983, *Geophys. Res. Lett., 11*, 745–748, 1984.

Richardson, P. L., and T. K. McKee, Average seasonal variation of the Atlantic equatorial currents from historical ship drifts, *J. Phys. Oceanogr., 14*, 1226–1238, 1984.

Schumacher, A., Monatskarten der Oberflachenstromungen im Nordatlantischen Ozean (5°S–50°N), *Ann. Hydrogr. Mar. Meteorol., 68*, 109–123, 1940.

Schumacher, A., Monatskarten der Oberflachenstromungen im aquatorialen und sudlichen Atlantischen Ozean, *Ann. Hydrogr. Mar. Meteorol., 71*, 209–219, 1943.

Weisberg, R. H., L. Miller, A. Horigan, and J. A. Knauss, Velocity observations in the equatorial thermocline during GATE, *Deep Sea Res., 26*, suppl. 11, 217–248, 1979.

Wyrtki, K., Sea level and the seasonal fluctuations of the equatorial currents in the western Pacific Ocean, *J. Phys. Oceanogr.*, *4*, 91–103, 1974.

Wyrtki, K., Sea level during the 1972 El Niño, *J. Phys. Oceanogr.*, *7*, 779–789, 1977.

Wyrtki, K., The response of the sea surface topography to the 1976 El Niño, *J. Phys. Oceanogr.*, *9*, 1223–1231, 1979.

S. Arnault, Laboratoire d'Océanographie Dynamique et de Climatologie, Office de la Recherche Scientifique et Technique Outre-Mer, Université Pierre et Marie Curie, T14-2, 4 place Jussieu, 75252 Paris Cedex 05, France.